IEEE Photonics Journal
An IEEE Photonics Society Publication

Open Access

Efficient 2D Optical Beamforming Network With Sub Partitioning Capability Based on Raised Cosine Chirped Fiber Grating and Mach-Zehnder Delay Interferometer

Volume 13, Number 3, June 2021

Ritesh Kumar, *Student Member, IEEE*
Sanjeev Kumar Raghuwanshi, *Senior Member, IEEE*

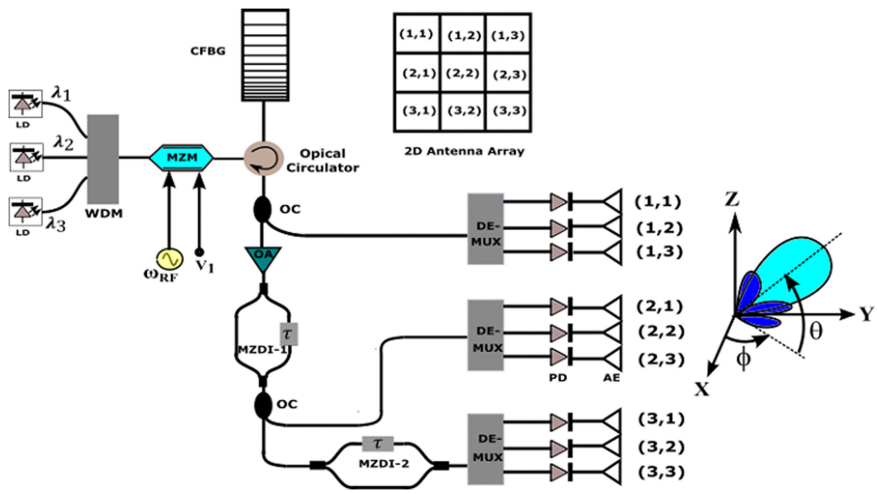

DOI: 10.1109/JPHOT.2021.3082185

Efficient 2D Optical Beamforming Network With Sub Partitioning Capability Based on Raised Cosine Chirped Fiber Grating and Mach-Zehnder Delay Interferometer

Ritesh Kumar,[1] ***Student Member, IEEE***,
and Sanjeev Kumar Raghuwanshi,[1] ***Senior Member, IEEE***

[1]Photonic Laboratory, Department of Electronics Engineering, Indian Institute of Technology (Indian School of Mines) Dhanbad, Dhanbad, Jharkhand 826004, India

DOI:10.1109/JPHOT.2021.3082185

Manuscript received April 10, 2021; revised May 10, 2021; accepted May 17, 2021. Date of publication May 20, 2021; date of current version June 4, 2021. This work was supported in part by the Indian Space Research Organization Project number: ISRO/(10)/2018-2019/571/ECE under Grants DS-2B-13 012(2)/13/2018 and ISRO/RES/3/775/19-20, in part by Space Applications Centre, Indian Space Research Orgainization, Ahmedabad, India with ISRO Respond project entitled "A novel Mach Zehnder Modulator based integrated photonic highly steerable beam-forming system for broadband satellite communication link", and in part by the Project number: ISRO/(10)/2018-2019/571/ECE under Grants DS-2B-13012(2)/13/2018 and ISRO/RES/3/775/19-20. Corresponding author: Ritesh Kumar (e-mail: ritesh.16DR000125@ece.ism.ac.in).

Abstract: In this paper, a two-dimensional true time delay optical beamforming network (OBFN) has been proposed with sub partitioning capability for 3X3 phased array antenna (PAA) with operating frequency in X-Band. The architecture is based on raised cosine apodised chirp fiber Bragg grating (CFBG) and Mach-Zehnder delay interferometer (MZDI). Compared to unapodised CFBG, raised cosine apodization drastically reduces the ripple as well as sidelobes and gives a flat response in the passband of reflection spectrum. Multiwavelength optical signals with a wavelength difference of 0.3 nm are used to steer 10 GHz RF signal in elevation and azimuth direction. Further, broad angular control of beam radiation due to sub partitioned PAA is also demonstrated. The RF signal beam is steered in elevation at -62.2,-31.9, and-10.8 degrees, and in azimuth at 123.6 and 55.9 degrees. Theoretical analysis of the OBFN has been presented and validated with the experimental results. At the best of our knowledge, delay characteristics of raised cosine apodised CFBG have been theoretically explored for the first time with mathematical formulation and a comparative discussion is given with the measured data.

Index Terms: Chirped fiber Bragg grating, Mach-Zehnder interferometer, optical beamforming network, true-time delay, two dimensional angular control.

1. Introduction

THE high demand for phased array antennas (PAA) in remote sensing applications, which can be used to tune the direction of transmission and reception of microwave signals. [1]. It is also capable of generating simultaneously multiple beams of microwave signals. However, the performance of PAA is highly affected by the characteristics of beam forming network (BFN) in terms of electromagnetic interference (EMI), frequency of operation, and phase tuning [2]. Whereas electronic BFN has a limited instantaneous bandwidth, lacks tunability in angular control of the

beam, and cannot feed a large array of antennas. These limitations can be overcome by BFN based on optical components. The optical BFN has some built-in advantages, such as EMI immunity, squint-free beam transmission, low power consumption, and light weight [3].

In the past few decades, the optical beamforming network (OBFN) based on different optical delay components has taken great attention for its implication in beam steering with PAA [4]–[10]. OBFN based on ring resonators (RRs) provides sufficient range of delay with the tuning optical carrier frequency [4], [5], but the cascading of numerous RRs may result in a large ripple in delay characteristics. In [6], [7], multiple number of chirp fiber Bragg gratings (CFBGs) were used to demonstrate a variable optical delay line. OBFN based on Polarization domain interferometers avoid the need for multiple numbers of CFBG using several polarization controllers [8]. In [9], multiple optical signals are individually modulated by external modulators and dedicated to photonic crystal fiber of unique length. These techniques are committed to one dimensional phased array antenna where elevation control of RF beam is well represented. However, two directional angular control of RF beam, where beam steering can be controlled in elevation as well as azimuth direction [11]–[13],have the ability to scan targets in multiple directions in remote sensing applications. Ref. [11] describes multiwavelength OBFN for two dimensional PAA based on fabricated hardware compressive architecture of delay element, where a large number of RRs have been integrated on a single chip. Two dimensional PAA with wide radiation direction shows the capability of subarray partitioning which is based on cascading of fiber Bragg gratings and commercially available variable delay lines [12]. In this technique, two CFBGs with a reflection bandwidth of 5 nm were used.But, no theoretical details regarding delay and reflection of CFBG have been discussed with the variation in wavelength. In ref [13], a tunable filter is required at each antenna element, which may make the system complex and costly. Overall, costs, size, power usage, and complexity related to the number of components required for scalable broadband and large arrays are key drawbacks limiting the practical implementation of these techniques in real life. Recently, the authors have also proposed photonic techniques for the generation of microwave signals and investigated their applications in beam steering [14] and remote sensing area [15], [16].

In the present article, a two-dimensional optical delay network is proposed based on raised cosine apodized CFBG and Mach-Zehnder delay interferometer (MZDI). The proposed OBFN is employed to 3X3 PAA, which provides squint free broad angular control of RF beams in the elevation and azimuth direction. Multiwavelength optical signals are passed through CFBG, which provides delay between horizontally placed antenna elements of the PAA. After CFBG, a part of multiwavelength signals is further processed through MZDI to introduce delay between vertically placed antenna elements of the PAA. Further, theoretical analysis of the OBFN has been represented and validated with the experimental results. With the best knowledge of authors, delay characteristics of raised cosine apodized CFBG have been theoretically explored first time with mathematical formulation and also a comparative discussion is made with the measured data. Furthermore, the proposed technique reduces the optical components in terms of modulators and delay elements, minimising complexity and power requirements.

2. Theory

An optical beam forming network has been proposed for two-directional beam steering of RF signal in X-Band. A schematic diagram of the proposed architecture is shown in Fig. (1). Multiwavelength laser sources are used in Fig. (1) to provide optical carriers with wavelengths λ_1, λ_2, and λ_3. These optical carriers are optically combined through Wavelength Division Multiplexer (WDM). An RF signal of ω_{RF} frequency is generated by a function generator and used to modulate optical signal of ω frequency. Here, the Mach-Zehnder modulator (MZM) operates as an intensity modulator where the number of frequency components present in the modulated signal can be limited by the smaller value of the modulation index. The MZM has been set to operate in a linear region with low RF power and its bias voltage has been set for quadrature transmission point. A small value of modulation index (β) has been taken which gives double sideband (DSB) modulation by MZM. After DSB modulation, the modulated optical signal is passed through raised cosine apodized

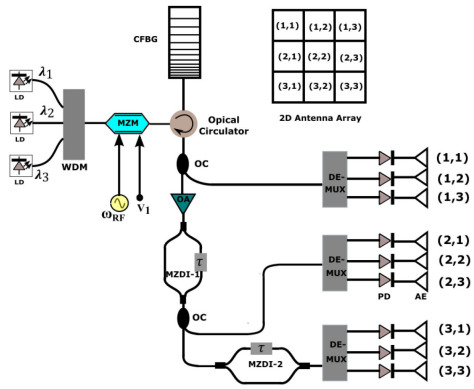

Fig. 1. Schematic diagram of the proposed optical beamforming network for 3X3 rectangular antenna array.

chirp fiber Bragg grating (CFBG) of reflectivity $R(\omega) = |R(\omega)|e^{j\phi(\omega)}$. Where, $|R(\omega)|$ is the intensity of reflection and $\phi(\omega)$ is the phase change due to reflection by CFBG. The reflected modulated signal at the output of CFBG contains $R(\omega)$, $R(\omega - \omega_{RF})$, and $R(\omega + \omega_{RF})$ which appear due to the DSB modulation. The reflected optical signal from CFBG can be written as [17]

$$x_i(t) = \frac{E_o}{\sqrt{2}}\Big[J_0(\beta)\left|R_i(\omega)\right| e^{j\phi_i(\omega)}e^{j\omega t} + J_{-1}(\beta)\left|R_i(\omega-\omega_{RF})\right| e^{j\phi_i(\omega-\omega_{RF})} \times e^{j(\omega-\omega_{RF})t}$$
$$+J_1(\beta)\left|R_i(\omega+\omega_{RF})\right| e^{j\phi_i(\omega+\omega_{RF})}e^{j(\omega+\omega_{RF})t}\Big] \quad (1)$$

One of the split parts of the reflected signal from optical coupler (OC) is passed through a wavelength de-multiplexer (DE-MUX) and detected by the photodetector (PD) to the excite first row of antenna array (AA). The remaining part of the reflected signal is optically amplified by an optical amplifier (OA) and passed through Mach-Zehnder delay interferometer (MZDI) to introduce further delay in excitation for the rest portion of AA. This has been discussed later in this section. Photocurrent detected by i^{th} PD employed for the first row of AA is given by

$$I_{1,i}(t) = I_{1,i}(\omega_{RF}, \omega)e^{j(\omega_{RF}t + \psi_{1,i}(\omega_{RF},\omega))} \quad (2)$$

where magnitude $I_{1,i}(\omega_{RF}, \omega)$ and phase $\psi_{1,i}(\omega_{RF}, \omega)$ of photocurrent $I_{1,i}(t)$ can be found in [17]. In the equations of magnitude and phase response, DC term and higher order harmonics have been neglected due to band pass nature of PD and smaller value of modulation index. Consider that CFBG has large reflection bandwidth compared to the RF signal bandwidth, then $|R_i(\omega)| \approx |R_i(\omega - \omega_{RF})| \approx |R_i(\omega + \omega_{RF})|$ and $\phi_i(\omega + \omega_{RF}) - \phi_i(\omega) \approx \phi_i(\omega) - \phi_i(\omega - \omega_{RF})$. The approximated amplitude and phase response have given in equations (3) and (4), respectively.

$$I_{1,i}(\omega_{RF}, \omega) = 2\left|R_i(\omega)\right|^2 \quad (3)$$

$$\psi_{1,i}(\omega_{RF}, \omega) = -\tau_{1,i}(\omega) \cdot \omega_{RF} \quad (4)$$

where $\tau_{1,i}(\omega) = -\frac{d\phi_i(\omega)}{d\omega_{RF}}$ represents wavelength dependent delay due to reflection from CFBG, theoretical analysis of delay due to CFBG is discussed in subsection 2.1. It should be noted here that $\tau_{1,i}(\omega)$ is column wise delay induced between adjacent antenna elements (AEs) of PAA.

Array factor (AF) for the first row of PAA is given by

$$AF_x(\theta) = \sum_{i=0}^{N-1} I_{1,i}(\omega_{RF}, \omega)e^{j(\psi_{1,i}(\omega_{RF},\omega) + i\omega_{RF}.dx.\frac{\sin\theta}{c})} \quad (5)$$

In equation (5), θ is the radiation angle of the beam in elevation direction, dx is the distance between AEs, and c is the speed of light in free space.

2.1. Delay Analysis of CFBG

Consider a linear chirp fiber grating of length L and grating chirp function $\varphi(z)$ which depends on the distance along axis of fiber core i.e., $\varphi(z) = \varphi_0 - (z - \frac{L}{2}) \cdot \frac{\Delta}{L}$. Here, φ_0 is the nominal period of grating defined at the center of grating length and Δ is the total chirp which is much smaller than φ_0. In CFBG, refractive index $\delta n(z)$ is not uniform and it changes along the propagation direction of light. We have considered raise cosine refractive index profile which is expressed as

$$\delta n(z) = \frac{\bar{\delta n}}{2}\left(1 + \cos\left(\frac{\pi z}{L}\right)\right) \tag{6}$$

$\delta n(z)$ is the perturbation profile to the effective refractive index n_{eff} of the grating which helps to select the apodization of CFBG, and $\bar{\delta n}$ is the average value of DC index change over the grating period. In coupled mode differential equations, AC coupling coefficient $K(z)$ and DC coupling coefficient $\bar{\sigma}(z)$ have taken based on equations (7) and (8), respectively [18].

$$K(z) = \frac{\pi \upsilon}{\lambda}\delta n(z) \tag{7}$$

$$\bar{\sigma}(z) = 2\pi n_{eff}\left(\frac{1}{\lambda} - \frac{1}{\lambda_D}\right) + \frac{2\pi}{\lambda}\delta n(z) - \frac{1}{2}\cdot\frac{\Delta}{L} \tag{8}$$

where n_{eff} is the effective refractive index of fiber core, λ_D denotes design wavelength, and υ represents fringe visibility of index change. Expression of reflection coefficient for uniform grating with constant coupling coefficient has been shown in [18]. In the present paper, coupled mode differential equations with varying coupling coefficients define in equations (7) and (8) have considered and mathematically solved to obtain the expression of delay due to CFBG. The derived expression of delay has been shown in (9).

$$\tau = \frac{1}{2\pi c}\cdot f_1(\lambda, z)\cdot\left[f_2(z)\cdot f_3(\lambda, z)\cdot\frac{1}{\lambda} + f_3(\lambda, z)\cdot f_4(\lambda, z) + f_5(\lambda, z)\right] \tag{9}$$

where

$$f_1(\lambda, z) = \frac{\bar{\sigma}^2(z)}{\bar{\sigma}^2(z) + (K^2(z) - \bar{\sigma}^2(z)).\coth^2\left(\sqrt{K^2(z) - \bar{\sigma}^2(z)}\cdot L\right)} \tag{10}$$

$$f_2(z) = 8\pi^2(n_{eff} + \delta n(z))^2 - 2(\pi\upsilon\delta n(z))^2 \tag{11}$$

$$f_3(\lambda, z) = \frac{1}{2\bar{\sigma}(z)}\cdot\left[\frac{\coth\left(\sqrt{K^2(z) - \bar{\sigma}^2(z)}\cdot L\right)}{\sqrt{K^2(z) - \bar{\sigma}^2(z)}} - L\cdot csch^2\left(\sqrt{K^2(z) - \bar{\sigma}^2(z)}\cdot L\right)\right] \tag{12}$$

$$f_4(\lambda, z) = 8\pi^2(n_{eff} + \delta n(z))\left(\frac{1}{4\pi}\cdot\frac{\Delta}{L} - \frac{n_{eff}}{\lambda_D}\right) \tag{13}$$

$$f_5(\lambda, z) = \frac{2\pi\cdot(n_{eff} + \delta n(z))\cdot\sqrt{K^2(z) - \bar{\sigma}^2(z)}}{\bar{\sigma}^2(z)} \times \coth\left(\sqrt{K^2(z) - \bar{\sigma}^2(z)}\cdot L\right) \tag{14}$$

Equation (9) represents the analytical expression for delay of any chirp FBG. The delay characteristics of CFBG with raised cosine apodization has been shown in Fig (2(a)). This characteristic has been plotted for the delay expression represented by (9), where $\bar{\delta n}$ is 1×10^{-4}, φ_0 is 170.21×10^{-9} m, L is 1 cm, and υ is 1. It can be seen from Fig. (2(a)) that delay variation is almost linear with constant slope of 61.25 ps/nm in the wavelength range 1553 nm to 1553.9 nm. Reflection characteristics having the same parameters of raised cosine apodized CFBG is shown in Fig. (2(b)). In Fig. (2(b)), normalized reflectivity is depicted for different reflecting wavelengths in the range of 1550-1556 nm where maximum reflectivity of flat response was found in wavelength range 1553 nm to 1553.9 nm. This gives 0.9 nm reflection bandwidth of CFBG. A linear variation in delay

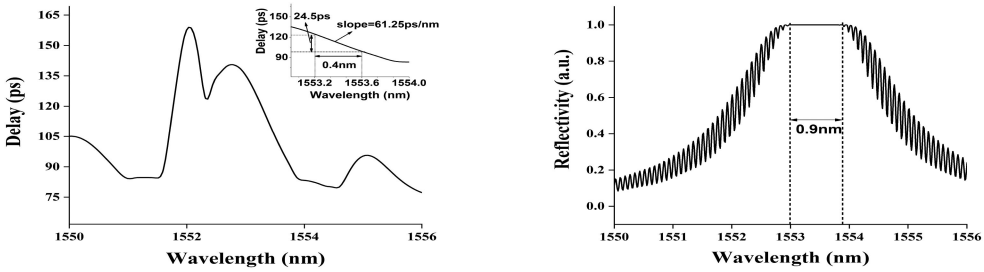

(a) (b)

Fig. 2. (a) Delay characteristics of raised cosine apodized CFBG (b) Reflectivity of the raised cosine apodized CFBG.

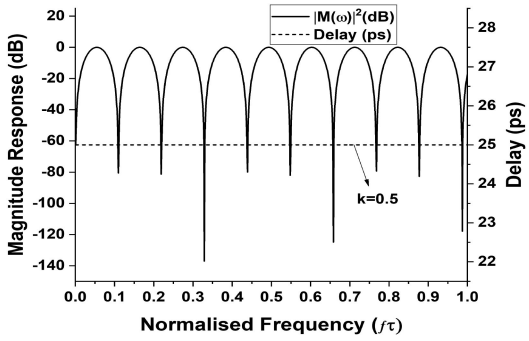

Fig. 3. Magnitude response $|M(\omega)|^2$ (left y-axis) and delay response (right y-axis) of MZDI.

was also found in the same range of reflecting wavelengths which gives sufficient relative delay among multiwavelength optical signals. For example, a step difference of 0.3 nm in wavelengths can have a progressive delay of 18.4 ps in beam steering by 3X3 PAA.

2.2. Delay Analysis of MZDI

MZDI is used as the delay element to provide delay between vertically placed AEs in 3X3 PAA i.e., it introduces progressive delay between two consecutive rows of the PAA. Transfer function of MZDI can be found based on its input-output relation and using only one input port of MZDI with 3-dB coupler (coupling coefficient, $k = 0.5$) and lossless phase shift section, it can be expressed as

$$M(\omega) = \frac{e^{j\Phi_2}}{2} \cdot (e^{j\Delta\Phi} - 1) \tag{15}$$

Here, Φ_1 and Φ_2 are the respective phase induced in the upper and lower arms of MZDI. Phase difference between these two arms is $\Delta\Phi = \Phi_1 - \Phi_2 = \omega\tau$ where ω is the angular frequency of propagating signal, and $\tau = \frac{\Delta L}{v_g}$ is the time delay due to differential path length (ΔL) and group velocity v_g of the propagating wave inside the waveguide of MZDI. Magnitude response of the above transfer function can be written as

$$\left|M(\omega)\right|^2 = \frac{1}{2} \cdot (1 - \cos(\omega\tau)) \tag{16}$$

where $\omega = 2\pi f$ and $f\tau$ denotes the normalized frequency. Magnitude response and delay due to MZDI has been shown in Fig. (3). It can be observed from Fig. (3) that the magnitude response

$|M(\omega)|^2$ (left y-axis) has very much narrower stopband than free spectral range at less than -80 dB, and group delay (right y-axis) is 25 ps for the power coupling coefficient $k = 0.5$ at all normalized frequency.

2.3. Array Factor of 3X3 PAA

A part of reflected signal from CFBG is given to one of the input ports of MZDI-1 as depicted in Fig. (1). It will introduce additional delay of τ_y due to the difference in path lengths between two arms of MZDI-1. Delayed optical signal can be written as

$$\begin{aligned} y_i(t) = & \left|R_i(\omega)\right| \cdot \left|M_i(\omega)\right| \cdot e^{j(\Phi_i(\omega)+\theta_i(\omega))} \cdot e^{j\omega t} \\ & + \left|R_i(\omega-\omega_{RF})\right| \cdot \left|M_i(\omega-\omega_{RF})\right| \cdot e^{j(\Phi_i(\omega-\omega_{RF})+\theta_i(\omega-\omega_{RF}))} \times e^{j(\omega-\omega_{RF})t} \\ & + \left|R_i(\omega+\omega_{RF})\right| \cdot \left|M_i(\omega+\omega_{RF})\right| \times e^{j(\Phi_i(\omega+\omega_{RF})+\theta_i(\omega+\omega_{RF}))} \cdot e^{j(\omega+\omega_{RF})t} \end{aligned} \tag{17}$$

where $\theta_i(\omega)$ is the argument of $M_i(\omega)$. Performing similar analysis as previously done for CFBG, a part of delayed optical signal is passed through de-multiplexer (DE-MUX) and detected by the photodetector (PD) to excite second row of AA. Photocurrent detected by i^{th} PD employed for exciting second row of AA is given by

$$I_{2,i}(t) = I_{2,i}(\omega_{RF}, \omega) e^{j(\omega_{RF} t + \psi_{2,i}(\omega_{RF}, \omega))} \tag{18}$$

where $I_{2,i}(\omega_{RF}, \omega)$ and $\psi_{2,i}(\omega_{RF}, \omega)$ can be found in [17]. Consider that bandwidth offered by the delay elements is much higher than the bandwidth of modulating signal, then $\phi_i(\omega+\omega_{RF}) + \theta_i(\omega+\omega_{RF}) - \phi_i(\omega) - \theta_i(\omega) \approx \phi_i(\omega) + \theta_i(\omega) - \phi_i(\omega-\omega_{RF}) - \theta_i(\omega-\omega_{RF})$. Therefore, the phase of detected photocurrent can be approximated as

$$\begin{aligned} \psi_{2,i}(\omega_{RF}, \omega) &= \phi_i(\omega+\omega_{RF}) - \phi_i(\omega) + \theta_i(\omega+\omega_{RF}) - \theta_i(\omega) \\ &= -[\tau_{1,i}(\omega) + \tau_y] \cdot \omega_{RF} \end{aligned} \tag{19}$$

In equation (19), $\tau_{1,i}(\omega)$ is the delay provided along x-direction of rectangular AA, whereas τ_y is the additional delay along y-direction for the second row of rectangular AA. With the same condition of bandwidth considered in phase approximation, the amplitude response can also be approximated as

$$I_{2,i}(\omega_{RF}, \omega) = 2[\left|R_i(\omega)\right| \cdot \left|M_i(\omega)\right|]^2 \tag{20}$$

Remaining part of optical signal available at the output port of MZDI-1 is passed through MZDI-2 to have a progressive delay τ_y in the excitation for the third row of AA. Phase of photocurrent detected by i^{th} PD employed for the third row of AA is

$$\psi_{3,i}(\omega_{RF}, \omega) = -[\tau_{1,i} + 2\tau_y] \cdot \omega_{RF} \tag{21}$$

Consider a two-dimensional grid of planar surface for the case of NXM rectangular array of AEs. Here, AEs are placed in XY-plane with interelement spacing of dx and dy along x and y axes, respectively. Position vector of $(n, m)^{th}$ AE is given by$r_{nm} = n \cdot dx \cdot a_x + m \cdot dy \cdot a_y$; $n = 1, 2, 3$ and $m = 1, 2, 3$, a_x and a_y are the unit vectors along x and y axes, respectively. Array factor of two dimensional PAA is given by [1]

$$AF(\theta, \phi) = \sum_{m=1}^{M} \sum_{n=1}^{N} I_{m,n}(t) e^{jk_0 a_r \cdot r_{nm}} \tag{22}$$

In the above equation (22), $I_{m,n}(t)$ provides amplitude and phase excitation to the $(n, m)^{th}$ AE, k_0 is the propagation constant, and $a_r = \sin\theta\cos\phi a_x + \sin\theta\sin\phi a_y + \cos\theta a_z$ is unit vector along the radiating direction in free space. Where, θ is inclination angle and ϕ represents azimuth angle of

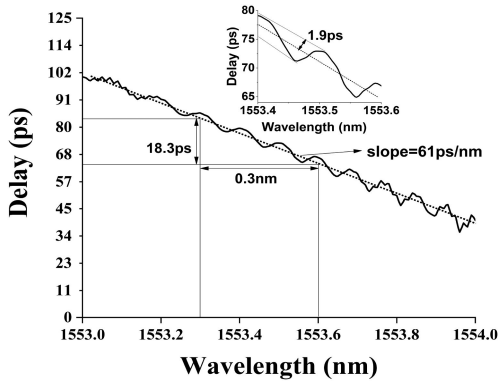

Fig. 4. Delay characteristics of the CFBG measured for wavelength ranges 1553 nm to 1554 nm.

the radiating beam. For the present analysis array factor of 3X3 PAA can be written as

$$AF(\theta,\phi) = \sum_{m=1}^{3}\sum_{n=1}^{3} I_{m,n}(\omega_{RF},\omega) \times e^{j(\psi_{m,n}(\omega_{RF},\omega)+\frac{(n\cdot dx\cdot\cos\phi+m\cdot dy\cdot\sin\phi)\cdot\sin\theta\cdot\omega_{RF}}{c})} \tag{23}$$

3. Result and Analysis

A tunable multiwavelength laser source (Model Number: OSICS ECL 1560 Tunable laser module) is used to get optical carrier signal whose wavelength is varied from 1553 nm to 1553.6 nm with wavelength tuning step of 0.3 nm. The multiwavelength optical carrier signal is intensity modulated by RF signal of 10 GHz frequency and 1.42 V amplitude with the help of MZM (Model Number: IMC-1550-20-PM). Half wave voltage of the MZM is 6 V and a bias voltage of 1.1 V is applied at its bias port through modulator driver (Model Number: MD-20-M OPTILAB). An RF signal of 10 GHz frequency has taken from function generator (Aligent Technologies E8257D) and applied at the RF port of MZM through the modulator driver. The modulated optical signal is then passed to raised cosine apodised CFBG which is fabricated in our collaborative lab. To select the apodization, the average refractive index is kept constant along the length of the grating while the refractive index modulation amplitude is gradually changed. Here, grating writing requires a double scan operation. In the first scan, the UV beam passes through the phase mask and writes the grating into the fiber. The UV beam's intensity varies as it scans along the fiber to establish an apodization profile. After removing the phase mask with direct illumination, the UV beam is screened along the fiber again. The UV beam intensity varies over time in comparison to the first scan, ensuring that every point of the grating receives the same total UV dose in both scans. Delay characteristics of the CFBG has been measured for the wavelength ranges 1553 nm to 1554 nm and has shown in Fig. (4). From Fig. (4), a linear variation of delay with small magnitude ripples has observed for continuous change in wavelength ranges 1553 nm to 1554 nm. In this wavelength range, a constant slope of 61 ps/nm has found which introduce maximum error of 1.9 ps, shown in the inset of Fig. (4). There has been found a good agreement between simulated and measured result of delay variation in the wavelength range of 1553 nm to 1554 nm.

This delay variation has been applied in the excitation available to each PDs of 20 GHz bandwidth employed for the horizontally placed AEs of any row i.e., column wise relative delay has been introduced by the CFBG. Fig. (5(a)) represents delayed RF signals carried by multiwavelength optical carrier signal at 1553 nm, 1553.3 nm, and 1553.6 nm. These RF signals have detected by the respective PDs which are employed for the first row of AA. Progressive relative delay measured between consecutive AEs of the first row are found to be 21 ps and 43 ps. The measured data has little deviation from theoretical value due to the presence of small ripples in the delay characteristics of CFBG. MZDI was used to have a progressive delay between two consecutive rows of antenna

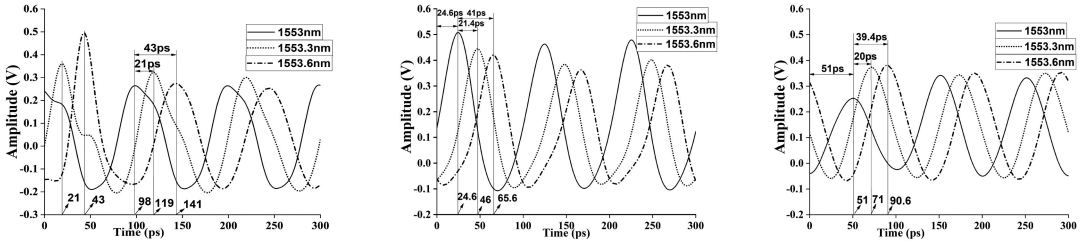

(a) (b) (c)

Fig. 5. Delayed RF signal of corresponding optical wavelengths 1553 nm, 1553.3 nm, and 1553.6 nm due to (a) CFBG (b) CFBG and MZDI-1 and (c) CFBG, MZDI-1, and MZDI-2.

array for any column. MZDI-1 introduces 25 ps delay between all AEs of first and second rows for a given column. The delayed RF signal detected by PDs employed for the second row of AA has shown in Fig.(5(b)). It can be observed from Fig. (5(b)) that RF signal at 1553 nm, 1553.3 nm, and 1553.6 nm has additional delay of 24.6 ps for the second row of AA in comparison to first row of AA. In the present case, progressive relative delay between pair of consecutive AEs placed in the second row of AA, are found to be 21.4 ps and 41 ps. The measured data is very less affected by delay ripples. Another MZDI (MZDI-2) is placed before PDs for third row of AA. Due to the presence of MZDI-2, it is supposed to have an additional delay of 25 ps for all AEs placed in the third row of AA. Delayed RF signals available at different optical wavelengths have been depicted in Fig. (5(c)). In Fig. (5(c)), relative delay between RF signals for the first and third row of AA is found to be 51 ps. This result holds for any column of the AA. The obtained delay has a deviation of 1 ps from the predicted value of 50 ps which shows good approximation of theoretical data. For the AEs of third row, measured values of progressive relative time delays are 20 ps, and 39.4 ps. From the above discussion it can be noticed that CFBG has used for the delay (τ_x) between horizontally placed AEs, however MZDI has used for the delay (τ_y) between vertically placed AEs of 3X3 AA.

The obtained delayed RF signals have been investigated in beam steering to observe the radiation pattern formed by 3X3 AA. The proposed architecture of OFBN gives two directional delay variation, therefore, beam steering is possible in vertical (θ) and azimuthal direction (ϕ). such kind of radiation pattern has two directional angular control which is highly attractive in military and airborne applications. The maximum operating frequency of each AE is 16 GHz. To avoid grating lobes, distance between consecutive AEs (d) should follow the relation $\frac{d}{\lambda} < \frac{1}{1+|\cos\psi_0|}$ i.e., $d < \lambda(1 - \frac{\alpha_n}{2\pi n})$. Here, λ is operating wavelength of RF signal, ψ_0 is the beam angle in the direction of maximum radiation, α_n is the phase shift due to delay in excitation of n^{th} antenna. In the fabricated antenna array, interspacing of consecutive AEs is $d = 3$ mm. First for the reference, we have demonstrated radiation pattern by 3X3 AA without considering any delay in the excitations of AEs i.e., $\tau_x = \tau_y = 0$.

Fig. (6) shows the radiation pattern of entire antenna array without processing any delay in RF signals. Fig. (6(a)) depicts three-dimensional representation of radiation pattern by 3X3 AA, which is the function of θ and ϕ. In the present case, maximum radiation is found in the direction at beam pointing angle $(\theta_0, \phi_0) = (0^o, 0^o)$ where sidelobes of the radiation pattern are well suppressed compare to the main lobe. Fig. (6(b)) and Fig. (6(c)) shows respective variation in beam pattern radiated by entire AA for $\phi = 0$ plane and $\theta = 0$ direction. 3 dB beamwidth in $\phi = 0$ and $\theta = 0$ direction is found to be $\theta_{3^-dB} = 52^o$ and $\phi_{3^-dB} = 103^o$, respectively.

Next, we have investigated the radiation pattern formed by different sub partitioned AA. Fig. (7) depicts radiation pattern in terms of normalised array factor formed due to the sub partitioned 1X3 AA where both theoretical and experimental delay values have been considered. Fig. (7(a)) represents the same in inclination direction i.e., θ ranges -90^o to 90^o, and maximum radiation in the inclination direction was found at θ equal to -62.2^o. The measured value of 3 dB beam width of the main lobe is 41.5^o. Fig. (7(b)) shows the radiation pattern in azimuth direction i.e., ϕ

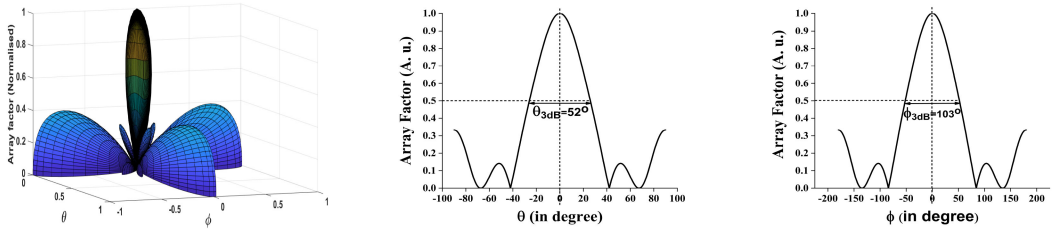

(a) (b) (c)

Fig. 6. Radiation pattern of 3X3 antenna array for zero delayed RF signals (a) three dimensional (θ and ϕ are scalled by π) (b) along $\phi = 0$ plane (c) along $\theta = 0$ direction.

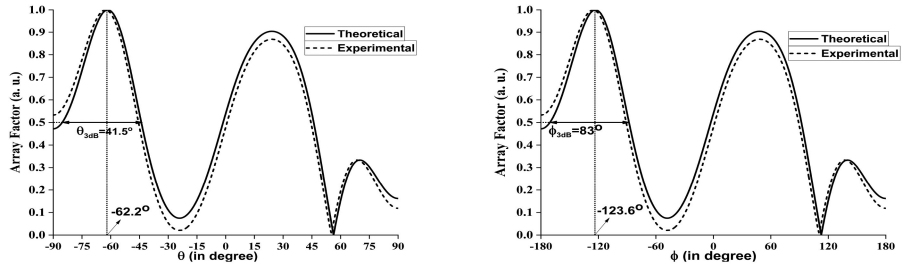

(a) (b)

Fig. 7. Radiation pattern of 1X3 subarray AEs (a) along vertical direction (θ) and (b) along azimuthal direction (ϕ).

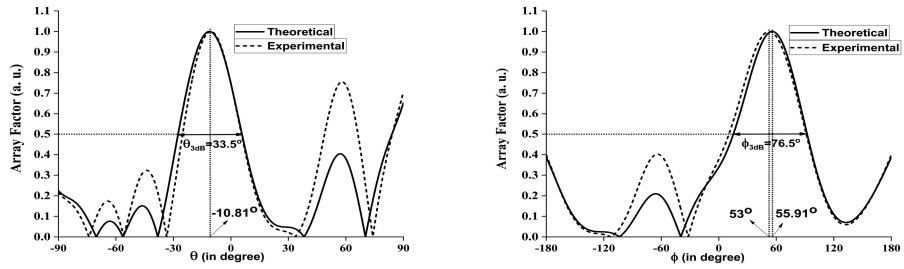

(a) (b)

Fig. 8. Radiation pattern of 2X3 subarray AEs (a) along vertical direction (θ) and (b) along azimuthal direction (ϕ).

ranges -180^o to 180^o, and maximum radiation in this direction was found at ϕ equal to -123.6^o. The 3 dB beam width of main lobe in azimuth direction was found to be 83^o. In Fig. (7), Solid line representation of radiation pattern has been drawn for the theoretical values of delay whereas dashed line representation of radiation pattern has been shown for experimental values of delay. Fig. (7(a)) and Fig. (7(b)) show good agreement between theoretical and experimental results.

In our next discussion, radiation pattern formed due to the sub partitioned 2X3 AA has been explored and the consistent results have shown in Fig. (8). In this case, relative delay of 24.6 ps (experimental value) and 25 ps (theoretical value) has been introduced between the excitations available for the AEs placed in first and second row of 2X3 AA. This has been made possible through MZDI-1. Relative delay between horizontally placed consecutive AEs in a particular row are only due to the CFBG. Fig. (8(a)) represents the radiation pattern in inclined direction whereas Fig (8(b)) shows the same in azimuth direction. In Fig. (8(a)), maximum radiation in the direction

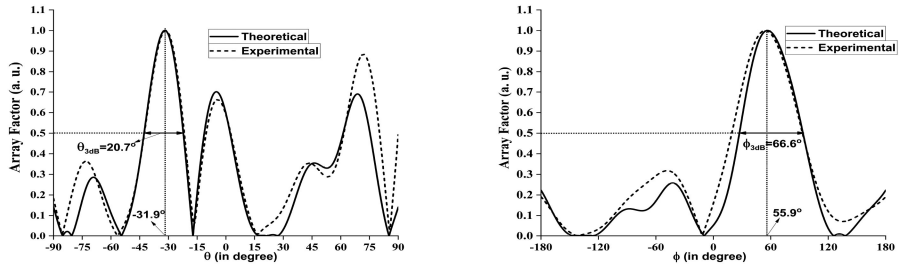

Fig. 9. Radiation pattern of 3X3 subarray AEs (a) along vertical direction (θ) and (b) along azimuthal direction (ϕ).

TABLE 1
Delay Provided to Each Row of Antenna Array and Their Beam Angles

Size of Antenna Array $(i \times j)$	Horizontal Delay (in ps) $(\tau_{x,i})$ $(i = 1, 2, 3)$	Vertical Delay (in ps) (τ_y)	Direction of maximum radiation (θ, ϕ)	3dB beamwidth of main lobe $(\theta_{3dB}, \phi_{3dB})$
1×3	$0, 21, 43$	0	$(-62.2^o, 123.6^o)$	$(41.5^o, 83^o)$
2×3	$24.6, 46, 65.6$	24.6	$(-10.8^o, 55.9^o)$	$(33.5^o, 76.5^o)$
3×3	$51, 71, 90.6$	51	$(-31.9^o, 55.9^o)$	$(20.7^o, 66.6^o)$

of inclination was found at θ equal to -10.81^o, this holds true for both theoretical and experimental data. The measured value of 3 dB beam width of the main lobe was found to be 33.5^o. However, in Fig. (8(b)), maximum radiation in azimuthal direction was found at ϕ equal to 53^o and 55.91^o for experimental and theoretical value of relative delay, respectively. This difference has occurred due to the presence of small nonuniformity in experimental data. The 3 dB beam width of the main lobe in azimuth direction is 76.5^o.

Finally, radiation pattern of entire 3X3 AA is calculated and shown in Fig. (9). This radiation pattern has been achieved by applying horizontal progressive relative delays of 20 ps and 39.4 ps in the excitation of third row. The vertical progressive relative delays between excitation of two consecutive rows of the AA have been considered as 24.6 ps and 51 ps. Fig. (9(a)) shows normalised array factor in the vertical direction and maximum radiation intensity was found for θ equal to -31.9^o. Main lobe has 3 dB beam width of 20.7^o in inclination direction. Fig. (9(b)) represents the beam steering of RF signal in azimuth direction, and the maximum radiation intensity is found to be located at ϕ equal to 55.9^o which has 3 dB beam width of 66.6^o.

The experimental results obtained in above discussions have been summarized in Table-1. It represents progressive horizontal delays ($\tau_{x,i}$) for the AEs placed in the i^{th} row of AA, vertical delays ($\tau_{y,j}$) for the j^{th} row of AA. It also represents the direction of maximum radiation in terms of inclination and azimuth angles with their 3 dB beam width for the sub partitioned AA.

4. Conclusions

Two directional beam steering of 10 GHz RF signal in X-Band has been proposed and demonstrated by true time delay optical beamforming network for 3X3 PAA. The presented architecture contains raised cosine apodized CFBG and MZDI, which introduces wavelength dependent delay for multiwavelength optical signals. This gives squint free beam steering of the RF signal in elevation direction at-62.2,-31.9 and-10.8 degrees, and azimuth direction at 123.6 and 55.9 degrees. 3 dB beamwidth of radiating beam for each sub partitioned PAA has also been discussed and narrower beamwidth has been achieved with an increase in the size of the antenna array. Theoretical analysis of the OBFN has been conducted and validated by the experimental results.

Obtained delay characteristics of raised cosine apodized CFBG have been theoretically explored for the first time with mathematical formulation and a comparative discussion is given with the measured data. The two directional angular control in beam radiation is highly attractive in military and airborne applications.

Acknowledgement

The Authors would like to thanks Mr R K Bahl, Head, Optical Communication Division, Satcom and Navigation Payload Area, Space Application Centre, Indian Space Research Organization (ISRO), Ahmedabad 380053, for necessary experimental support.

References

[1] C. A. Balanis, *Antenna Theory: Analysis and Design*. Hoboken, NJ, USA: Wiley, 2016.
[2] R. J. Mailloux, *Phased Array Antenna Handbook*. Norwood, MA, USA: Artech House, 2017.
[3] H. Zmuda and E. N. Toughlian, *Photonic Aspects of Modern Radar*. Norwood, MA, USA: Artech House, 1994.
[4] L. Zhuang, C. Roeloffzen, R. Heideman, A. Borreman, A. Meijerink, and W. van Etten, "Single-chip ring resonator-based 1 optical beam forming network in CMOS-compatible waveguide technology," *IEEE Photon. Technol. Lett.*, vol. 19, no. 15, pp. 1130–1132, Aug. 2007.
[5] P. A. Morton and J. B. Khurgin, "Microwave photonic delay line with separate tuning of the optical carrier," *IEEE Photon. Technol. Lett.*, vol. 21, no. 22, pp. 1686–1688, Nov. 2009.
[6] D. B. Hunter, M. E. Parker, and J. L. Dexter, "Demonstration of a continuously variable true-time delay beamformer using a multichannel chirped fiber grating," *IEEE Trans. Microw. Theory Techn.*, vol. 54, no. 2, pp. 861–867, Feb. 2006.
[7] N. K. Srivastava, R. Parihar, and S. K. Raghuwanshi, "Efficient photonic beamforming system incorporating a unique featured tunable chirped fiber bragg grating for application extended to the ku-band," *IEEE Trans. Microw. Theory Techn.*, vol. 68, no. 5, pp. 1851–1857, May 2020.
[8] M. V. Drummond, P. P. Monteiro, and R. N. Nogueira, "Photonic true-time delay beamforming based on polarization-domain interferometers," *J. Lightw. Technol.*, vol. 28, no. 17, pp. 2492–2498, 2010.
[9] H. Subbaraman, M. Y. Chen, and R. T. Chen, "Photonic crystal fiber-based true-time-delay beamformer for multiple rf beam transmission and reception of an x-band phased-array antenna," *J. Lightw. Technol.*, vol. 26, no. 15, pp. 2803–2809, 2008.
[10] C. Tsokos, E. Mylonas, P. Groumas, L. Gounaridis, H. Avramopoulos, and C. Kouloumentas, "Optical beamforming network for multi-beam operation with continuous angle selection," *IEEE Photon. Technol. Lett.*, vol. 31, no. 2, pp. 177–180, Jan. 2019.
[11] M. Burla *et al.*, "Multiwavelength-integrated optical beamformer based on wavelength division multiplexing for 2D phased array antennas," *J. Lightw. Technol.*, vol. 32, no. 20, pp. 3509–3520, 2014.
[12] B. Ortega, J. Mora, and R. Chulia, "Optical beamformer for 2D phased array antenna with subarray partitioning capability," *IEEE Photon. J.*, vol. 8, no. 3, Jun. 2016, Art. no. 6600509.
[13] L. Gao and K. H. Wagner, "Wavelength-compensated photonic multibeam-forming system for two-dimensional wide-band radio-frequency phased-array antennas," *Appl. Opt.*, vol. 48, no. 22, pp. E 1-E12, 2009.
[14] R. Kumar and S. K. Raghuwanshi, "Simultaneous photonic generation of multiple chirp and unchirp microwave waveform with frequency multiplying capability for optical beam forming system," *Opt. Quantum Electron.*, vol. 51, no. 11, p. 344, 2019.
[15] R. Kumar and S. K. Raghuwanshi, "A photonic scheme for the generation of dual linear chirp microwave waveform based on the external modulation technique and its airborne application," *Opt. Quantum Electron.*, vol. 49, no. 11, p. 370, 2017.
[16] R. Kumar and S. K. Raghuwanshi, "Photonic generation of a parabolic-shaped microwave signal and dual-linear-chirp microwave waveform," *Appl. Opt.*, vol. 59, no. 20, pp. 6024–6029, 2020.
[17] B. Ortega, J. L. Cruz, J. Capmany, M. V. Andrés, and D. Pastor, "Variable delay line for phased-array antenna based on a chirped fiber grating," *IEEE Trans. Microw. Theory Techn.*, vol. 48, no. 8, pp. 1352–1360, Aug. 2000.
[18] T. Erdogan, "Fiber grating spectra," *J. Lightw. Technol.*, vol. 15, no. 8, pp. 1277–1294, 1997.